The Cryosphere Discuss., 9, 4205–4235, 2015
www.the-cryosphere-discuss.net/9/4205/2015/
doi:10.5194/tcd-9-4205-2015

The Cryosphere Discussions
Open Access

Fram Strait spring ice export and September Arctic sea ice

M. H. Halvorsen[1], L. H. Smedsrud[1,2,3], R. Zhang[4], and K. Kloster[5]

[1]Geophysical Institute, University of Bergen, Bergen, Norway
[2]Bjerknes Center for Climate Research, Bergen, Norway
[3]University Centre in Svalbard, Longyearbyen, Norway
[4]Geophysical Fluid Dynamics Laboratory, National Oceanic and Atmospheric Administration, Princeton, NJ 08540, USA
[5]Nansen Environmental and Remote Sensing Center, Bergen, Norway

Received: 1 July 2015 – Accepted: 21 July 2015 – Published: 7 August 2015

Correspondence to: L. H. Smedsrud (larsh@gfi.uib.no)

Published by Copernicus Publications on behalf of the European Geosciences Union.

Abstract

The Arctic Basin exports ~ 10 % of the sea ice area southwards annually through Fram Strait. A larger than normal export decreases the remaining mean thickness and ice area. A new updated timeseries from 1979–2013 of Fram Strait sea ice area export shows an overall increase until today, and that more than 1 million km^2 has been exported annually in recent years. The new timeseries has been constructed from high resolution radar satellite imagery of sea ice drift across 79° N from 2004–2013, regressed on the observed cross-strait surface pressure difference, and shows an increasing trend of 7 % per decade. The trend is caused by higher southward ice drift speeds due to stronger southward geostrophic winds, largely explained by increasing surface pressure on Greenland. Spring and summer area export increases more (~ 14 % per decade) than in autumn and winter, and these export anomalies have a large influence on the following September mean ice extent.

1 Introduction

Along with expectations for a warming planet, the Arctic sea ice cover continues to decrease. During the last two decades the Arctic sea ice cover has become both thinner and smaller in extent (Comiso, 2012; Stroeve et al., 2012). In September 2012 the lowest observed September sea ice extent (SIE) since the satellite record started in 1979 occurred. The 2012 minimum was 18 % lower than in 2007, and 49 % below the 1979–2000 average minimum (Cavalieri et al., 1996, updated yearly). A number of processes have been suggested to explain parts of the sea ice loss, such as differences in surface air temperatures, the poleward advection of heat in both the ocean and atmosphere, greenhouse gas forcing, and cloud cover.

Changes in ice export is also considered an important contributor to variability in the Arctic sea ice cover (Nghiem et al., 2007; Smedsrud et al., 2011). Historically, about 10 % of the Arctic sea ice area is exported through Fram Strait annually, and the ice

export through the other Arctic gateways are on an order of magnitude smaller (Kwok, 2009). Because quite thick ice is lost this way (Hansen et al., 2013) a larger than normal export decreases the remaining mean thickness in addition to the sea ice covered area inside the Arctic Basin.

Recent studies on sea ice motion have shown that sea ice drift speed is increasing in the Arctic Basin (Hakkinen et al., 2008; Rampal et al., 2009), and in Fram Strait (Rampal et al., 2009; Smedsrud et al., 2011). Positive trends were also found in cumulative Fram Strait ice area export by Widell et al. (2003) (4 % per decade in the period 1950–2000) and Smedsrud et al. (2011) (5 % per decade in the period 1957–2010). Contrary to these studies, Kwok et al. (2013) found a small negative trend in cumulative Fram Strait ice area export in the similar period 1982–2009, but with positive trends for both annual (October–September) and summer (June–September) from 2001–2009. Spreen et al. (2009) did not observe any significant change in Fram Strait ice volume export for the period 2003–2008.

The Arctic seasonal maximum sea ice cover occurs in late February or early March (Zwally and Gloersen, 2008). Ice export through Fram Strait between March and August could therefore influence the following September SIE, because sea ice is mostly melting within the Arctic Basin during these months (Smedsrud et al., 2011; Kwok and Cunningham, 2010). However, such an influence has not been found so far. Our new timeseries shows such an influence, and suggests that high accuracy monitoring of the Fram Strait ice area export should be continued and would contribute to seasonal forecasts of the next September SIE. This paper focuses on the continued high level of area export and the relation between spring and summer sea ice export and the following September Arctic SIE.

2 Data and methods

In this study we used observed sea ice drift speed onwards from February 2004 and updated through December 2013. The drift is calculated by recognising displacement vectors manually on Envisat Advanced Synthetic Aperture Radar (ASAR) WideSwath and Radarsat-2 ScanSAR (from 2012) images captured 3 days apart (Kloster and Sandven, 2014). Displacement vectors that cross 79° N were linearly interpolated to bins (1° longitude, each 21 km) from 15° W to 5° E (Fig. 1). For most 3 days image pairs, displacement vectors with an accuracy of about ±3 km is found with a spacing of 30–50 km. This accuracy of about ±3 km per vector is considered sufficient for most analysis. This is because subsequent averaging or addition in time/space of many unbiased vectors will generally result in ice mean speed and ice export values with a significantly better accuracy than 10 %. We only use the monthly mean cross-strait value of ice drift speed here, being the spatial-temporal mean southward speed of all ice crossing 79° N (Fig. 1) between the fast ice edge and the pack ice edge at 50 % concentration. On the western side of the strait a linear interpolation from zero motion in the stable fast ice to the first measured motion vector is made. It is assumed that ice displacement to the east of the last measured vector is constant near the ice edge. The mean speed value results from the averaging of about 50 individual, unbiased displacement vectors, thus the calculated mean speed value should be considerably more accurate than 10 %.

Ice area export over consecutive 3-day-periods along 79° N is a product of sea ice drift data and passive microwave sea ice concentration data (Kloster and Sandven, 2014). We use cumulative (monthly and yearly) ice area export onwards from 2004. From here on ice area export will be referred to as ice export.

Observed monthly mean Sea Level Pressure (mSLP) values were used onwards from 1979. The cross-strait difference along 78° N was then calculated between 18° W and 15° E. Monthly mSLP observations was obtained from Longyearbyen (Fig. 1, Svalbard Airport, Norwegian Meteorological Institute, http://eklima.met.no). On the Greenland side surface pressure at 18° W was constructed using weighted average of monthly mSLP from two nearby stations; Danmarkshavn and Nord (Fig. 1, Danish Meteorological Institute, Cappelen, 2014). mSLP from Danmarkshavn and Nord correlated well (r = 0.94) and allowed calculations of cross-strait geostrophic winds fol-

lowing Thorndike and Colony (1982), and correlations and linear regressions between this wind and observed sea ice drift speed or ice export.

We used National Snow and Ice Data Center ice extent since 1979 (Cavalieri et al., 1996, updated yearly). The ice extent is defined as the area covered by ice greater than 15 % ice concentration, and has been derived from Scanning Multichannel Microwave Radiometer (SMMR) and Special Sensor Microwave/Imager (SSM/I) brightness temperatures using the NASA Team sea ice algorithm.

A coupled climate model (Geophysical Fluid Dynamics Laboratory Coupled Model version 2.1 (GFDL), Delworth et al., 2006) is used to further investigate the coupling between sea ice export and September Arctic SIE. In the ocean the model has 50 vertical levels and 1° zonal resolution. Its atmosphere component has 24 vertical levels, with horizontal resolution of 2° latitude × 2.5° longitude. We mostly utilize a 3600 year control simulations were the model is forced by constant radiative conditions representative of 1860. This produces a stable multi-millennium control integration without flux adjustments, that simulate most features of the relationship between atmospheric/oceanic forcing and Arctic sea ice cover realistically (Zhang, 2015).

3 Results and discussion

The most dominant forces acting on sea ice are the wind drag and the ocean drag (Thorndike and Colony, 1982). On short time scales (from days to months), geostrophic winds alone explain above 70 % of the variance of the ice speed in the Arctic Ocean (Thorndike and Colony, 1982), and winds are also the dominant force acting on sea ice in Fram Strait (Widell et al., 2003). Here ice drift is in the south-southwesterly direction, and a mean southward speed of 16 cm s^{-1} has been reported based on moorings at 5° W in the period 1997–2000 (Widell et al., 2003). Figure 1 shows that the temporal mean speed is quite constant across the strait eastward of 5° W, and that the speed decreases westward towards the Greenland coast. Velocities are clearly strongest during winter, with mean speeds above 20 cm s^{-1} decreasing to less than 10 cm s^{-1} during

summer in the outer part (Fig. 1) The ice export occurs mostly between 5° W and the Greenwich Meridian. The export is limited on the western side by the decreasing ice speed, reaching zero at 16° W were stationary land fast ice is usually found, and by zero concentration on the eastern side varying from 5° W to 5° E (Fig. 1 in Smedsrud et al., 2011). Export estimates from passive satellites (Kwok, 2009) and those based on mSLP difference and SAR tracking are largely consistent for the 80's and 90's (Smedsrud et al., 2011).

3.1 Atmospheric forcing

From a linear regression between monthly mean ice drift speed and geostrophic wind we find that the ice in Fram Strait drifts at a speed being 1.6 % of the geostrophic wind speed (Eq. 1). The constant contribution resulting from the linear regression, which is the speed of the ice given no local wind forcing, is 6.5 cm s^{-1} (Eq. 1). Both terms are comparable to previous studies (Widell et al., 2003; Smedsrud et al., 2011; Thorndike and Colony, 1982). The standard error of the regression was 3.5 cm s^{-1}.

$$V_{\text{ice}} = 0.016 \times V_g + 0.065\,[\text{m s}^{-1}] \quad (1)$$

The constant contribution of 6.5 cm s^{-1} represents the mean (not wind-driven) ocean current. A nonlinear component of the ice drift including forces from variations in ocean currents or internal ice stress may also represent parts of this constant (Thorndike and Colony, 1982). The correlation between monthly mean ice speed and geostrophic wind was good, $r = 0.76$ with the 95 % confidence interval [0.67 0.83]. We also correlated the monthly mSLP with the maximum monthly sea ice drift speed along 79° N, which resulted in similar correlations. Analyzing the east-west variations showed that 33.0 % of the 1° longitude bins reached the monthly maximum speed. This means that maximum speed and mean speed relate to the wind forcing in the same way, and that the east-west averaging contains the variability. The correlation between Fram Strait cross-strait mSLP difference and ice export was $r = 0.73$.

3.2 Ice drift seasonality

The annual cycle of mSLP-based ice speed (and export) is similar to earlier estimates (Kwok, 2009), with higher speed during winter, and weaker during summer. Annual mean speed is close to 12 cm s^{-1} (Fig. 2). This mean value is a spatially avaraged value between 15 and 5° W, and a temporal average for the years 1979–2013. Based on the NCEP reanalysis data Smedsrud et al. (2011) found significantly lower mean ice speed in the 1960's and 1970's.

The previous assumption of a constant contribution throughout the year of 6.5 cm s^{-1} is challenged by our new results. We discovered a seasonal difference between the observed ice speed and the estimated mSLP-based speed (Fig. 2). The difference suggest that the ice speed should be 3.0 cm s^{-1} stronger during winter (December–April), and 2.8 cm s^{-1} weaker during summer (June–October). This is inconsistent with vartiations in the internal ice stress; ice is thicker and more dense during winter, resulting in a larger ice stress and thereby weaker ice drift speed for a similar wind. An increase in the mean ocean current below the ice during winter, which in this case is the East Greenland Current (EGC), is consistent with the generally stronger winds in the North Atlantic region during winter. This suggest that the EGC is responding to the larger scale windforcing as well as to the local winds. Generally the entire circulation along the continental slope of the Arctic Basin – Nordic Seas is driven by the wind-stress curl north of the Greenland-Scotland ridge (Isachsen et al., 2003). Two recent studies confirm that the EGC is stronger during winter and is responding to the large-scale wind stress curl in the Nordic Seas. It is thus likely that this is causing the additional winter export (Fig. 2). De Steur et al. (2014) analysed mooring data along 79° N between 1997 and 2009, and found that surface currents were below 5 cm s^{-1} during summer and 10–15 cm s^{-1} during winter, also varying in the east-west direction. Daniault et al. (2011) found a maximum in the flow in January and a minimum in July for the years 1992–2009 based on altimetry at 60° N, and that the vertical distribution remained constant over this time period.

Assuming a stronger EGC during winter, and weaker during summer, not related to the local winds, we re-calculated the timeseries using this seasonal difference, and the corrected ice speed fitted the observations in a much better way (Fig. 2). The same correction was made for the calculated ice export, so the summer values were decreased and the winter values increased accordingly (not shown). The seasonal correction improved the correlations between observed and mSLP-based ice drift (r = 0.88 for ice speed and r = 0.87 for ice export). This means that our new timeseries explains close to 80 % of the observed ice drift variability. The constant contribution from the EGC during summer makes up ∼ 34 % of the mean monthly summer ice export of 42.1 × 10^3 km^2, and the contribution during winter makes up ∼ 55 % of the mean winter export of 110.5 × 10^3 km^2 (not shown).

3.3 Annual mean ice export and trends: 1979–2013

Using this newly confirmed seasonal variation explained by the EGC, in addition to the local winds calculated from observed mSLP, we calculate the monthly mean ice export prior to 2004 when SAR images became available. Monthly mean Fram Strait ice export (Fig. 3) was produced by using the mSLP-based ice export including the seasonal correction from 1979–2003, and the observed ice export from 2004–2013. Previous studies (Smedsrud et al., 2011; Widell et al., 2003; Kwok, 2009) used reanalysis mSLP data, and our present study should therefore represent a more accurate estimation. We discovered systematic differences between the NCEP Fram Strait reanalysis mSLP data and observed mSLP in the recent years that we are not able to explain (not shown), and decided therefore to base the new ice export estimates solely on observed mSLP. Prior to 2004 we do not utilize observations of cross-strait variations in the width of the ice covered area, ice speed or ice concentrations, but base our ice export values solely on the regression equation found between observed mSLP from Longyearbyen, station Nord and Danmarkshavn (Fig. 1) and observed SAR ice export.

Figure 3 shows an increase for both annual and seasonal values. Hereafter we define annual ice export values as winter centered averages (September–August), winter export as averages from September through February, and spring export as averages from March through August. The long-term annual mean ice export is close to 880×10^3 km^2 year^{-1}, thus higher than previous studies suggest (Smedsrud et al., 2011; Widell et al., 2003; Kwok, 2009). Fluctuations from year to year are large, but the ice export has remained higher than the long-term mean since 2006 (Fig. 3). The annual mean export has been larger than 1000×10^3 km^2 year^{-1} since 2010.

A high positive trend of +7.0 % per decade is found for annual values from 1979 to 2013 (Fig. 3). This trend is consistent with increasing ice drift speed observed in the Arctic Ocean (Spreen et al., 2011; Rampal et al., 2009). The trend is largely produced by higher ice export during spring. The winter ice export trend is +3.4 % per decade, while the spring export trend is +13.9 % per decade over the 35 year long period (Fig. 3).

We find comparable trends for the entire period (1979–2013) and for those based on the observed mSLP only (1979–2003). The trends are somewhat lower in the early period, but remain positive (annual, winter, spring values are 3.5, 10.5 and 1.3 % per decade, not shown). This indicates that the overall ice export trend is related to the increase in mSLP across Fram Strait, and has gradually increased since 1979. The increase in export is due to stronger geostrophic winds, and for spring it is generated by an increase of 0.6 hPa per decade in the mSLP on Greenland. The mSLP on the Svalbard side has a slighly lower, negative trend. In the 1980's the spring export was approximately half of the winter export. The robust trend in spring export has resulted in a smaller seasonal difference in recent years, and since 2011 the two are close in magnitude (Fig. 3).

We note that other results (Kwok et al., 2013; Spreen et al., 2009) are consistent with ours for the 80's and 90's but differ in the period since 2004. This is when we have SAR based ice velocity data available, and we believe that the cause of the differences

lay in that the passive satellite observations are to coarse to resolve the high speed export events during winter (Smedsrud et al., 2011).

3.4 Recent annual export

The annual mean ice area export since 2010 is 1100×10^3 km^2 (Fig. 3). This high export means an overall increase in how much of the Arctic Basin ice cover is "lost" each year. The Arctic Basin covers an area of ~ 7.8 million km^2, and has been fully ice covered from November through May since 1979 until today. The annual ice export during the 1980's ($\sim 800 \times 10^3$ km^2) was 10 % of this winter ice covered area. However, during the last three years the annual ice export has increased to 14 % of this area, meaning a 40 % increase in the relative sea ice area export, or the large-scale divergence of the Arctic Basin sea ice cover. Further, an estimate of the new annual mean ice covered area inside the Arctic Basin is 7.0 million km^2. This is based on reduced monthly mean ice extent between June and October.

Using this updated annual mean Arctic Basin ice cover of 7.0 million km^2, the Fram Strait ice export has been 16 % of the area since 2010. This is a 60 % increase in relative sea ice area export since the 1980's, and is clearly connected with the overall Arctic sea ice decline. During winter the open water anomalies created within the basin are quickly refrozen, and one major effect of the increased ice export since 1979 has therefore been to contribute towards the overall observed thinning since the 1990's (Kwok and Rothrock, 2009).

3.5 Ice export and September Arctic sea ice cover

A larger than normal ice export decreases the sea ice cover directly inside the Arctic Basin by transporting sea ice out. While the open water anomalies inside the basin refreeze during winter, they may be further enhanced by positive feedback mechanisms during summer. This transition from winter and re-freezing, to summer and positive feedback, occurs gradually later in the year as one moves north, but melting will prevail

over most of the Arctic Basin onwards from May (Markus et al., 2009). In this section we will discuss the direct effect of ice export anomalies onwards from March. Altough there may be some re-freezing in March, April and May, the newly formed ice will be thin, have a thin snow cover, and therefore easily melt and deform. We therefore first summarize the export anomalies onwards from March, and note that the Arctic seasonal maximum SIE occurs in late February or early March. We thus summarize open water areas created by export onwards from March, and assume that they will contribute directly to open water areas in September the same year. The areas may not refreeze due to solar radiation and warmer air temperatures, or they may form thin ice that melts later in the summer. The indirect effect and the ice-albedo feedback will be discussed in the next section.

Previous examination of the contribution of summer (June–September) ice export to the loss of multiyear ice cover from 2005 to 2008 (Kwok and Cunningham, 2010) indicated a small contribution. Our results show something different. The annual spring ice export has been about 500×10^3 km^2 since 2008 (Fig. 4). This is a 100 % increase compared to the spring export in the early 1980's, so in recent years an additional ice export of $\sim 250 \times 10^3$ km^2 has occurred during spring. Over the same timeframe the September SIE has decreased $\sim 2500 \times 10^3$ km^2, so the increased spring export can directly explain about 10 % of the loss (Fig. 4).

The low September SIEs in 2007 and 2012 thus seems related to high spring export these years (Fig. 4). Likewise did the export decrease in 2013, and the September 2013 extent recovered. Overall the two series correlate well, with $r = -0.57$ for the un-trended values, and with $r = -0.38$ when the trends are removed. We return to the correlation values in Sect. 3.7. Not all high export events are followed by an anomalously low September SIE, for example in 1990 and 2000. One suggestion to explain the missing response for a high spring export and normal September SIE lies in the thickness variability and its interaction with the regional wind forcing within the Arctic Basin. The thinner ice cover in more recent years will more easily deform and compact given a convergent wind field, while in the past the thicker ice cover may resist such

wind forcing. The thickness in Fram Strait has thinned with about 1 m since 1992, and the average age of the exported ice has decreased from 3 to 2 years, but there are large year-to-year fluctuations (Hansen et al., 2014).

One suggested mechanism for the rapid decline in summer Arctic SIE is that a larger winter export could create more even and thin first year ice. This more even first year ice may have a larger fraction of melt ponds during summer. Schröder et al. (2014) found a strong correlation between simulated spring melt pond fraction and September Arctic SIE. We find that the correlation between winter ice export and the following September SIE is quite low. For un-trended values $r = -0.28$, and for de-trended values $r = -0.18$. The low increase in winter ice export over the last 35 years (3.4 % per decade) also suggest that summer ice loss and September SIE is not particularly sensitive to winter sea ice export.

3.6 Role of positive feedbacks

In addition to the direct contribution of about 10 % on the September SIE from spring export through Fram Strait, the loss may be further enhanced by positive feedback mechanisms during spring and summer. Of these the ice- albedo feedback (Perovich et al., 2007), is the best known, but a thinner ice cover will also have a smaller resistance towards wind forcing (Rampal et al., 2009) and more easily deform. Both amplifies anomalies in thinner ice cover and leads to more open water areas.

There are significant trends for the melt onset inside the Arctic Basin, and melt starts about 10 days earlier today than around 1980 (Markus et al., 2009). Melting generally starts in late May, but this does not mean that export anomalies have no effect until then. As noted by Markus et al. (2009) are early formations of open water areas important as it boosts the ice-albedo feedback. A positive export anomaly will lead to a positive solar heating anomaly because open water is created. We estimate the loss of sea ice due to the combined effect of increased ice export and the related ice-albedo feedback below. Weather the heat anomaly just prevents further growth or leads to direct melting is not specified.

The additional solar heating of the upper ocean due to increased ice export can be estimated from the incident solar irradiance, the change in surface albedo, and the change in open water area (Perovich et al., 2007). To estimate the additional solar heating we used the change in ice export from the beginning of this study period (1979–1981 average) to the most recent period (2011–2013 average). Between these two periods the additional open water area from increased ice export has increased ∼ 63, 105, 140, 155, 196, and 214 × 10^3 km^2 from March through August. The monthly mean solar radiation is ∼ 33, 142, 257, 302, 233 and 133 W m^{-2}, from March through August, observed at Russian North Pole drift stations (Table 1, Björk and Söderkvist, 2002). The relevant change in surface albedo can be estimated as 0.53, i.e. the difference between a (melting) sea ice albedo of 0.6, and an open water albedo of 0.07 (Perovich et al., 2007).

The additional open water areas between March and August lead to an additional solar heating of ∼ 2.44 × 10^{20} J. This extra heat is enough to melt or prevent growth of 0.800 × 10^3 km^3 of ice. Choosing a mean ice thickness of 1.5 m (Zygmuntowska et al., 2013) for the ice (melted or prevented from forming) suggests an effected ice area of 531 × 10^3 km^2. This is twice the size of the original spring export anomaly, and increases the effect of the spring export anomaly to almost 30 %. This value appears when using a recent September Arctic SIE value of ∼ 5000 × 10^3 km^2 (Fig. 4). If only the direct effect is used until June, and then the feedback is applied onwards the total effect still explains about 20 %.

3.7 Overall effect of spring export

The above physically based estimates stated a direct effect of about 10 % rising to 30 % when including the ice albedo feedback. This was however only accounting for the trends, or long term changes, while there is additional year to year variability of both September SIE and the spring export.

Because we expect the ice export to both influence the trend and the variability, we do not remove the trend initially. The overall correlation between annual spring

ice export and the following September mean SIE (1979–2013) is $r = -0.57$, with the 95 % confidence interval [−0.76 −0.29]. This means that the ice export explains 31 % of the variance in the mean September SIE. For the recent ten years (2004–2013) when our ice export values are directly observed by SAR and the Arctic sea ice cover has been thinner and more responsive the correlation is $r = -0.76$ (95 % confidence interval [−0.94 −0.26]). This means that 57 % of the variance can be explained for this period. This indicate a growing influence of the spring sea ice export in recent years.

Removing the linear trends results in a correlation $r = -0.38$, with the 95 % confidence interval [−0.63 −0.05]. This indicates that ∼ 14 % of the variance in the de-trended September SIE can be explained by the de-trended spring ice export. This shows clearly that the ice export influences the trend in September SIE, but in addition it also influences the year-to-year variability (Fig. 4). Again is there higher correlations for the more recent 2004–2013 period, with $r = -0.57$.

From a linear regression between annual spring Fram Strait ice export and mean September Arctic SIE (Fig. 5), we find that the September SIE is −7.3 times the spring ice export the same year. For an export anomaly of 100 × 10^3 km^2, the response is thus a loss of September SIE of around 700 × 10^3 km^2. In the above calculations we were able to explain a loss of ∼ 300 × 10^3 km^2 including the ice albedo feedback, so clearly there are also other contributors to the overall loss of September SIE. The slope of the curve is set mainly by the recent years when September SIE is below 6000 × 10^3 km^2 (Fig. 5), when we also found the higher correlation and variance explained.

We are lacking updated pressure observations from Greenland to extend our time-series consistently through 2014. However we note that the September minimum increased from 2013 to 2014, consistent with the 2014 spring export being 15 % lower than the spring export in 2013 (not shown). There is thus significant year-to-year variability and the spring export seems to have an increasingly important role to play in explaining this variability. The positive trend for earlier onset of melt (Markus et al., 2009) is also consistent with the higher correlation between the spring export and the September minimum for the last decade.

The total loss of September SIE, and also of Arctic sea ice loss for other months of the year, is driven by a number of factors. The sea ice export is only one of these factors, but one that seems to be largely overlooked until today. The major contributor to the overall loss is probably increased longwave radiation related directly to increased green house gases (Stroeve et al., 2012). In addition has increased Atlantic and Pacific ocean heat transport into the Arctic ocean likely contributed (Zhang, 2015), and atmospheric heat transport probably played a role in the overall thinning between the 1960's and the 1980's (Smedsrud et al., 2008). To further investigate the proposed link between spring sea ice export and the following September SIE we utilize fully coupled climate model simulations below.

3.8 Coupled climate model simulations

The 3600 year control simulation from the Geophysical Fluid Dynamics Laboratory (GFDL) Coupled Model version 2.1 presented in Zhang (2015) was further investigated here. This control simulation represents pre-industrial levels of greenhouse gases, and should represent the natural variability of forcing and response for the Arctic sea ice in a good way. The simulated long-term climatology of the annual mean Fram Strait ice area export is about 1457×10^3 km^2 year^{-1}. This ice export is higher than that of the long-term mean presented here (880×10^3 km^2 year^{-1}), but this is a common problem for many climate models (Langehaug et al., 2013). The standard deviation of simulated unfiltered spring Fram Strait ice area export is 327×10^3 km^2 year^{-1}, while the observed standard deviation is 83×10^3 km^2 year^{-1}. This difference is related to the much higher mean state in the model. The standard deviation of simulated 30 year low-pass filtered spring Fram Strait ice area export is 69×10^3 km^2 year^{-1}.

The main predictors of low-frequency variability of summer Arctic SIE was identified by Zhang (2015) as northward Atlantic heat transport, Pacific heat transport, and the spring Arctic Dipole (AD). Note that the time series used were 30 y low-pass filtered to extract the low-frequency variability. The ocean heat transport was calculated across the Arctic circle, and the simulation showed similar correlation between Arctic SIE and

ocean heat transport on the Atlantic and Pacific side ($r = -0.50$ and $r = -0.51$, both at 2 y lead).

The AD index is defined as the second leading mode (PC2) of spring (April–July) SLP anomalies within the Arctic Circle. Here a positive AD is defined as having a positive SLP anomaly over Greenland and a negative SLP anomaly over the Kara and Laptev Seas, which is efficient in causing enhanced transpolar ice drift. The AD influence on September Arctic SIE is strongest in spring, and we would like to investigate this influence further. Anomalous spring AD were significantly anticorrelated with the September Arctic SIE anomalies in the control simulation ($r = -0.37$ at 1 y lead for 30 year low-pass filtered anomalies, and $r = -0.41$ for unfiltered anomalies), and we believe that one of the main mechanisms for the AD's influence on September SIE is through the Fram strait ice export, which has increased significantly the last decade (Fig. 3). It is this pressure gradient that has increased and lead to stronger southerly winds in the Fram Strait. So an higher AD value leads to more ice being exported out of the Arctic Basin through Fram Strait. This relation between AD and ice cover anomalies has been noted both in observations and models (Wang et al., 2009; Overland et al., 2012), and is suggested to play a large role for future Arctic SIE variability (Wettstein and Deser, 2014). The simulated response is stronger in spring and summer and much weaker during autumn and winter (Zhang, 2015), consistent with the stronger correlation we found between September Aractic SIE and spring ice export than for the winter ice export.

Using the 3600 year long control simulation we find that the simulated spring Fram Strait ice export is indeed significantly correlated with the AD index, for both unfiltered ($r = 0.63$, Fig. 6) and 30 year low-pass filtered ($r = 0.59$, not shown) time series. This confirms this expected link between the overall atmospheric circulation and the Fram Strait export, also over much longer times than the last three decades when observations are available. In the simulations a larger correlation is found between the AD index and other months of spring export than March–August quoted above. For April–

August $r = 0.72$, and April-July ($r = 0.71$), this is reflecting the AD index defined for the April–July period as well.

For the unfiltered 3600 year simulation, spring Fram Strait ice area export also has an anti-correlation with the September Arctic SIE ($r = -0.34$, Fig. 7). This is similar to the correlation between AD and the September SIE of $r = -0.41$ mentioned above, suggesting that a substantial part of the coupling between the AD and the September SIE can be explained by the Fram Strait spring ice export. This $\sim 10\,\%$ of the total simulated variance in September SIE that can be explained by the spring export, is consistent with what we found for the observations when we de-trended the September SIE ($r = -0.38$). For the 30 year low-pass filtered time series, this correlation is lower ($r = -0.15$). This indicates that the spring export influences the September SIE mostly on yearly to decadal time scales, and that the lower frequencies (> 30 years) is dominated by the ocean heat transport. Similar correlations to $r = -0.34$ appear between the September SIE and the spring ice export when the export is evaluated over other months than March–August. Using April–August we found $r = -0.31$, and April–July $r = -0.32$, indicating that the main part of the signal is carried by the months of April–July.

Given that the control run only simulates natural climate variability we also investigated the observed AD anomalies since 1979 from the NCEP/NCAR reanalysis SLP dataset. As shown by Zhang (2015) is the observed September Arctic SIE anomaly anticorrelated with the the observed AD anomalies ($r = -0.53$). What is further added here is an explanation on how this link is physically working. The correlation between September SIE and the spring export was $r = -0.57$ (Fig. 4), so it provides a physical explanation for the AD correlation. The correlation is also slightly higher between the observed spring export and the September SIE, than for the observed AD and September SIE, but the difference is not significant. So if the goal is to explain September SIE variability the spring export is a more physical and stronger link than AD. Consistent with this view is the observed spring export and AD index also highly correlated ($r = 0.47$, Fig. 8). What further now has become clear is that the AD spring

export link also exist in the control simulation representing natural climate variability over 3600 years. As noted above was the correlation $r = 0.63$ between AD and spring export there.

We also examined a forced historical simulation for the 20th century combined with a forced 21th century projection under the CMIP3 A1B scenario using the GFDL model. Such a simulation is forced with changes in all external forcings such as anthropogenic greenhouse gases and aerosols. In these results we find no significant trend in simulated spring Fram Strait ice area export between 1979 and 2013. This suggests that the observed increase in spring Fram Strait ice area export since 1979 (Fig. 3) is not due to changes in anthropogenic external forcing, but due to internal natural variability.

4 Concluding remarks

A new and updated timeseries of Fram Strait ice area export from 1979–2013 was presented in this study. The new timeseries was constructed using high resolution radar satellite imagery of sea ice drift across 79° N from 2004–2013, regressed on the observed cross-strait surface pressure difference back to 1979. Stronger geostrophic winds, largely due to an observed increase in the surface pressure on Greenland, has created a high positive trend of 7 % per decade for annual mean ice area export since 1979 (Fig. 3). The trend is mostly explained by the high trends for spring and summer months, when ice export (March–August) has a robust trend of 13.9 % per decade.

The pressure difference from observed sea level pressure across the Fram Strait on Svalbard and Greenland directly explained 53 % of the variance in the observed ice export. The best fit between ice drift and geostrophic winds resulted in a seasonal difference of $\sim 3\,\mathrm{cm\,s^{-1}}$, suggesting that the ice drift is higher during winter, and lower during summer, than can be explained by local winds. The most likely explanation for this is a seasonal variation in the underlying East Greenland Current, driven by the large-scale wind forcing that are generally stronger during winter than summer. The seasonal cycle has also been confirmed by de Steur et al. (2014). The ice export

based on observed sea level pressure including a seasonal variation in the underlying current explains almost 80 % of the observed ice export variance.

The variability in sea ice area export is directly influencing the September Arctic sea ice cover. For de-trended time series 1979–2013, and for simulations over 3600 years with the GFDL coupled climate model, the Fram Strait spring ice area export explains about 10 % of the September SIE variability. This is explaining the previous noted link between the September SIE and the Arctic Dipole (Zhang, 2015), that show anti-correlations at the same level ($r = -0.41$) for the natural climate simulations. This influence is of the same order as the direct response of the increased spring ice area export, where an additional export of 250×10^3 km^2 between March and August in recent years, compares to about 10 % of the total loss of September SIE since 1980 (Fig. 4).

The sea ice area export influence on the September SIE also seems to have increased in recent years reflecting a thinner and more mobile sea ice cover. This influence is on the order of 30 % and appears from the plain correlation ($r = -0.57$), between not de-trended values of Fram Strait spring ice area export and the September SIE between 1979 and 2013. This link is also explaining the earlier noted correlations between the observed Arctic Dipole anomalies and the September SIE ($r = -0.53$, Zhang, 2015). One of the physical links is between Fram Strait ice export and September SIE, but this correlation and the one between September SIE and the Arctic Dipole, and the correlation between the Arctic Dipole and the Fram Strait export, are all on the level of $r = 0.5$. The increased influence can be explained by positive feedback mechanisms, such as the ice-albedo feedback and increased deformation of thinner ice, that further enhance such summer anomalies in SIE. Accounting for the ice-albedo feedback increases the observed annual increase in spring area export of 250×10^3 to 750×10^3 km^2, which is about 30 % of the observed September SIE loss.

The last 10 years the Arctic sea ice cover has decreased quite rapidly, and the contributions from natural and greenhouse gas forcing are still under debate. In our historical simulations we found no trend in Fram Strait sea ice export, and we are not aware of

results suggesting a likely systematic change in the Arctic large-scale circulation. We therefore find that the observed increase in ice export documented here is caused by natural climate variability, and that there is potential for a partial recovery of the Arctic September SIE in the future when, or if, the spring ice export decreases. The Arctic ice cover is now thinner and more mobile than before, and in the present state it seems to have an increased coupling to the Fram Strait ice area export. In the natural climate state this influence used to be on the order of 10 %, but during the last three decades the influence has increased to around 30 %.

Acknowledgements. Sea ice drift data was obtained from Kloster and Sandven (2014), where ScanSAR data has been provided by NCS/KSAT (Norwegian Space Center /Kongsberg Satellite Service) under the Norwegian-Canadian Radarsat agreements 2012–2014. Observed pressure data are from the Norwegian- and Danish Meteorological Institute. The observed Arctic Dipole index is derived from the NCEP/NCAR reanalysis, and the Arctic SIE data was obtained from the National Snow and Ice Data Center (NSIDC). This work was funded by the Geophysical Institute at the University of Bergen. We would like to thank Tor Gammelsrød for helpful comments.

References

Björk, G. and Söderkvist, J.: Dependence of the Arctic Ocean ice thickness distribution on the poleward energy flux in the atmosphere, J. Geophys. Res.-Oceans, 107, 37–1, 2002. 4217

Cappelen, J.: Weather observations from Greenland 1958-2013, Observation data with description, Tech. rep., DMI Technical Report 14-08, Danish Meteorological Institute, Copenhagen, 2014. 4208

Cavalieri, D., Parkinson, C., Gloersen, P., and Zwally, H.: Sea ice concentrations from Nimbus-7 SMMR and DMSP SSM/I passive microwave data, [1979–2013], Digital media, Boulder, Colorado USA, National Snow and Ice Data Center, available at: http://nsidc.org/data/nsidc-0051.html (last access: 15 October 2014), updated yearly, 1996. 4206, 4209

Comiso, J. C.: Large decadal decline of the Arctic multiyear ice cover, J. Climate, 25, 1176–1193, 2012. 4206

Daniault, N., Mercier, H., and Lherminier, P.: The 1992–2009 transport variability of the East Greenland-Irminger Current at 60 N, Geophys. Res. Lett., 38, L07601, doi:10.1029/2011GL046863, 2011. 4211

de Steur, L., Hansen, E., Mauritzen, C., Beszczynska-Möller, A., and Fahrbach, E.: Impact of recirculation on the East Greenland current in Fram Strait: results from moored current meter measurements between 1997 and 2009, Deep-Sea Res. Pt. I, 92, 26–40, 2014. 4222

Delworth, T. L., Broccoli, A. J., Rosati, A., Stouffer, R. J., Balaji, V., Beesley, J. A., Cooke, W. F., Dixon, K. W., Dunne, J., Dunne, K., Durachta, J. W., Findell, K. L., Ginoux, P., Gnanadesikan, A., Gordon, C. T., Griffies, S. M., Gudgel, R., Harrison, M. J., Held, I. M., Hemler, R. S., Horowitz, L. W., Klein, S. A., Knutson, T. R., Kushner, P. J., Langenhorst, A. R., Lee, H., Lin, S., Lu, J., Malyshev, S. L., Milly, P. C. D., Ramaswamy, V., Russell, J., Schwarzkopf, M. D., Shevliakova, E., Sirutis, J. J., Spelman, M. J., Stern, W. F., Winton, M., Wittenberg, A. T., Wyman, B., Zeng, F., and Zhang, R.: GFDL's CM2 global coupled climate models. Part I: Formulation and simulation characteristics, J. Climate, 19, 643–674, doi:10.1175/JCLI3629.1, 2006. 4209

Hakkinen, S., Proshutinsky, A., and Ashik, I.: Sea ice drift in the Arctic since the 1950s, Geophys. Res. Lett., 35, L19704, doi:10.1029/2008GL034791, 2008. 4207

Hansen, E., Gerland, S., Granskog, M., Pavlova, O., Renner, A., Haapala, J., Løyning, T., and Tschudi, M.: Thinning of Arctic sea ice observed in Fram Strait: 1990–2011, J. Geophys. Res.-Oceans, 118, 5202–5221, 2013. 4207

Hansen, E., Ekeberg, O.-C., Gerland, S., Pavlova, O., Spreen, G., and Tschudi, M.: Variability in categories of Arctic sea ice in Fram Strait, J. Geophys. Res.-Oceans, 119, 7175–7189, 2014. 4216

Isachsen, P. E., LaCasce, J., Mauritzen, C., and Häkkinen, S.: Wind-driven variability of the large-scale recirculating flow in the Nordic Seas and Arctic Ocean, J. Phys. Oceanogr., 33, 2534–2550, 2003. 4211

Kloster, K. and Sandven, S.: Ice motion and ice area flux in Fram Strait at 79N using SAR and passive microwave for Aug. 2004–Jul. 2014., Technical Report no. 322c, Nansen Environmental and Remote Sensing Center, Bergen, Norway, 2014. 4208, 4224

Kwok, R.: Outflow of Arctic Ocean sea ice into the Greenland and Barents Seas: 1979–2007, J. Climate, 22, 2438–2457, 2009. 4207, 4210, 4211, 4212, 4213

Kwok, R. and Cunningham, G. F.: Contribution of melt in the Beaufort Sea to the decline in Arctic multiyear sea ice coverage: 1993–2009, Geophys. Res. Lett., 37, L20501, doi:10.1029/2010GL044678, 2010. 4207, 4215

Kwok, R. and Rothrock, D.: Decline in Arctic sea ice thickness from submarine and ICESat records: 1958–2008, Geophys. Res. Lett., 36, L15501, doi:10.1029/2009GL039035, 2009. 4214

Kwok, R., Spreen, G., and Pang, S.: Arctic sea ice circulation and drift speed: decadal trends and ocean currents, J. Geophys. Res.-Oceans, 118, 2408–2425, 2013. 4207, 4213

Langehaug, H. R., Geyer, F., Smedsrud, L., and Gao, Y.: Arctic sea ice decline and ice export in the CMIP5 historical simulations, Ocean Model., 2013. 4219

Markus, T., Stroeve, J. C., and Miller, J.: Recent changes in Arctic sea ice melt onset, freezeup, and melt season length, J. Geophys. Res.-Oceans, 114, C12024, doi:10.1029/2009JC005436, 2009. 4215, 4216, 4218

Nghiem, S., Rigor, I., Perovich, D., Clemente-Colón, P., Weatherly, J., and Neumann, G.: Rapid reduction of Arctic perennial sea ice, Geophys. Res. Lett., 34, L19504, doi:10.1029/2007GL031138, 2007. 4206

Overland, J. E., Francis, J. A., Hanna, E., and Wang, M.: The recent shift in early summer Arctic atmospheric circulation, Geophys. Res. Lett., 39, L19804, doi:10.1029/2012GL053268, 2012. 4220

Perovich, D. K., Light, B., Eicken, H., Jones, K. F., Runciman, K., and Nghiem, S. V.: Increasing solar heating of the Arctic Ocean and adjacent seas, 1979–2005: attribution and role in the ice-albedo feedback, Geophys. Res. Lett., 34, L19505, doi:10.1029/2007GL031480, 2007. 4216, 4217

Rampal, P., Weiss, J., and Marsan, D.: Positive trend in the mean speed and deformation rate of Arctic sea ice, 1979–2007, J. Geophys. Res.-Oceans, 114, C05013, doi:10.1029/2008JC005066, 2009. 4207, 4213, 4216

Schröder, D., Feltham, D. L., Flocco, D., and Tsamados, M.: September Arctic sea-ice minimum predicted by spring melt-pond fraction, Nature Clim. Change, 4, 353–357, 2014. 4216

Smedsrud, L. H., Sorteberg, A., and Kloster, K.: Recent and future changes of the Arctic sea-ice cover, Geophys. Res. Lett., 35, L20503, doi:10.1029/2008GL034813, 2008. 4219

Smedsrud, L. H., Sirevaag, A., Kloster, K., Sorteberg, A., and Sandven, S.: Recent wind driven high sea ice area export in the Fram Strait contributes to Arctic sea ice decline, The

Cryosphere, 5, 821–829, doi:10.5194/tc-5-821-2011, 2011. 4206, 4207, 4210, 4211, 4212, 4213, 4214
Spreen, G., Kern, S., Stammer, D., and Hansen, E.: Fram Strait sea ice volume export estimated between 2003 and 2008 from satellite data, Geophys. Res. Lett., 36, L19502, doi:10.1029/2009GL039591, 2009. 4207, 4213
Spreen, G., Kwok, R., and Menemenlis, D.: Trends in Arctic sea ice drift and role of wind forcing: 1992–2009, Geophys. Res. Lett., 38, L19501, doi:10.1029/2011GL048970, 2011. 4213
Stroeve, J. C., Kattsov, V., Barrett, A., Serreze, M., Pavlova, T., Holland, M., and Meier, W. N.: Trends in Arctic sea ice extent from CMIP5, CMIP3 and observations, Geophys. Res. Lett., 39, L16502, doi:10.1029/2012GL052676, 2012. 4206, 4219
Thorndike, A. and Colony, R.: Sea ice motion in response to geostrophic winds, J. Geophys. Res.-Oceans, 87, 5845–5852, 1982. 4209, 4210
Wang, J., Zhang, J., Watanabe, E., Ikeda, M., Mizobata, K., Walsh, J. E., Bai, X., and Wu, B.: Is the Dipole Anomaly a major driver to record lows in Arctic summer sea ice extent?, Geophys. Res. Lett., 36, L05706, doi:10.1029/2008GL036706, 2009. 4220
Wettstein, J. J. and Deser, C.: Internal variability in projections of twenty-first-century Arctic sea ice loss: role of the large-scale atmospheric circulation, J. Climate, 27, 527–550, 2014. 4220
Widell, K., Østerhus, S., and Gammelsrød, T.: Sea ice velocity in the Fram Strait monitored by moored instruments, Geophys. Res. Lett., 30, 1982, doi:10.1029/2003GL018119, 2003. 4207, 4209, 4210, 4212, 4213
Zhang, R.: Mechanisms for low-frequency variability of summer Arctic sea ice extent, P. Natl. Acad. Sci. USA, 112, 4570–4575, 2015. 4209, 4219, 4220, 4221, 4223
Zwally, H. J. and Gloersen, P.: Arctic sea ice surviving the summer melt: interannual variability and decreasing trend, J. Glaciol., 54, 279–296, 2008. 4207
Zygmuntowska, M., Rampal, P., Ivanova, N., and Smedsrud, L. H.: Uncertainties in Arctic sea ice thickness and volume: new estimates and implications for trends, The Cryosphere, 8, 705–720, doi:10.5194/tc-8-705-2014, 2014. 4217

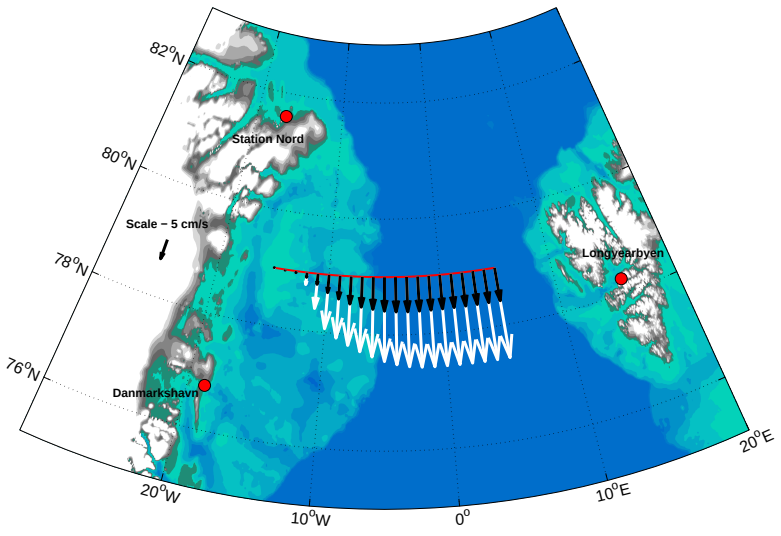

Figure 1. The Fram Strait between Greenland (left) and Svalbard (right) with summer (black arrows) and winter (white arrows) mean sea ice drift speed. Southward ice drift across 79° N (red line) from February 2004 to December 2013 were interpolated to 1° bins based on SAR imagery. Red circles show locations for surface pressure observations on Svalbard (Longyearbyen) and Greenland (Station Nord and Danmarkshavn). Pressure observations were interpolated between the Greenland stations to calculate the mean pressure gradient along 78.25° N. Summer means speeds are means over June–September, while winter speeds are December–March means. Shades of blue show ocean bathymetry in 100 steps down to 500 m depth.

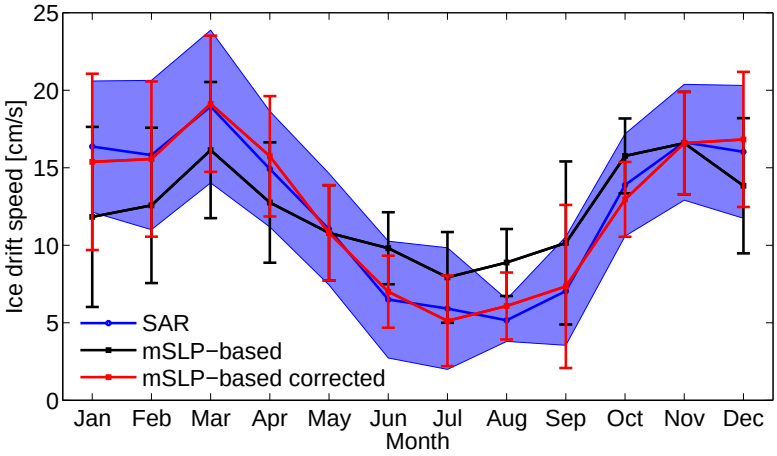

Figure 2. Annual cycle of monthly mean southward ice drift speed in Fram Strait. Observed ice drift speed (SAR) are shown in blue, and our pressure based ice drift speed in black. The corrected ice drift speed is shown in red. Standard deviations of observed ice drift speed are shaded in purple, and of calculated ice drift speed as vertical, coloured lines. All values are averaged from 2004–2013.

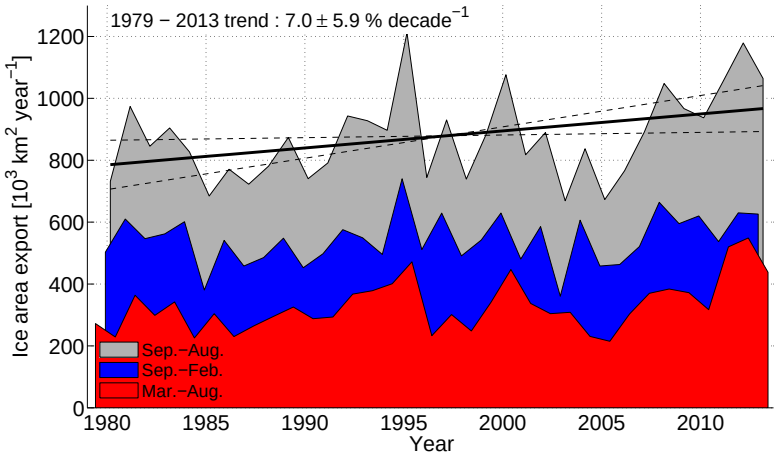

Figure 3. Annual southward ice area export in Fram Strait. Ice export from 1979–2003 is based on the relationship between observed mean sea level pressure and observed ice export by SAR, and ice export from 2004–2013 are solely observations by SAR. Annual values (grey) are averaged for 1 September through 31 August. Winter export is September–February (blue) and spring is March–August (red). Time averages are plotted half way through the respective period. The annual long-term linear trend is indicated (solid black line), and dashed lines indicate the 95 % confidence interval of the trend.

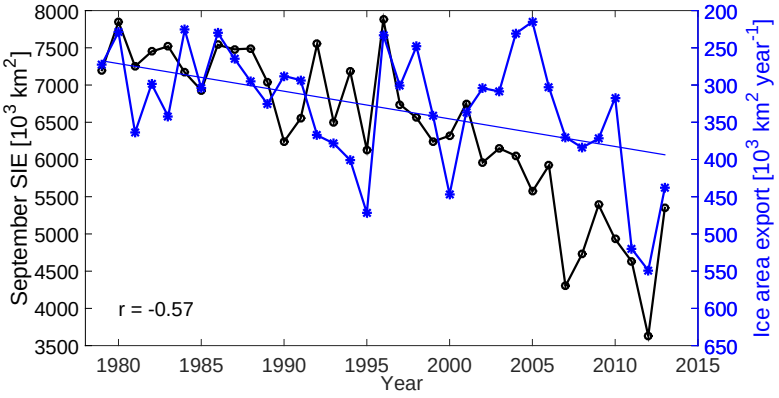

Figure 4. Spring Fram Strait ice area export (blue) and mean September Arctic SIE (black). The ice export is averaged for 1 March through 31 August. The *y* axis for the ice export is reversed for easier comparison. The reversed long-term linear trend in ice export (+13.9 % decade^{-1}) is shown in solid blue. SIE values are obtained from the National Snow and Ice Data Center.

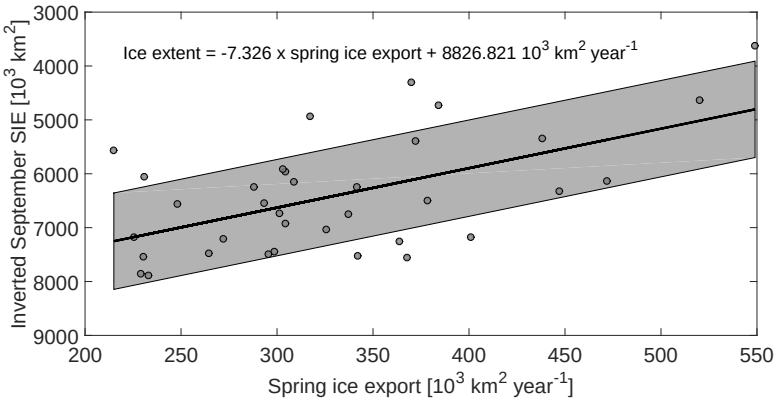

Figure 5. Linear fit between observed mean September Arctic SIE (NSIDC) and spring (March–August) Fram Strait ice area export. The shaded area is the standard error estimate of the linear fit.

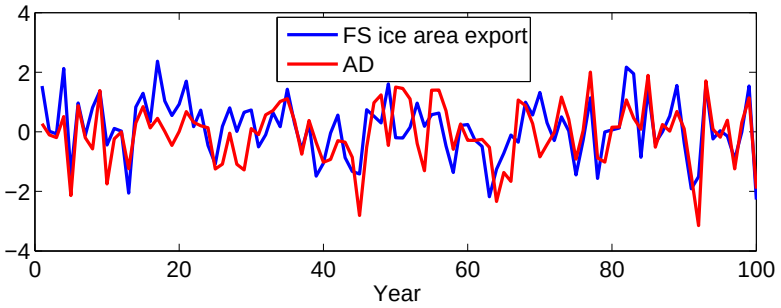

Figure 6. Spring Fram Strait (March–August) ice area export and Arctic Dipole anomaly from the 3600 year long control simulation. Both time series are unfiltered and normalized by their standard deviations. Only the first 100 years is shown. The correlation between the two series is $r = 0.63$.

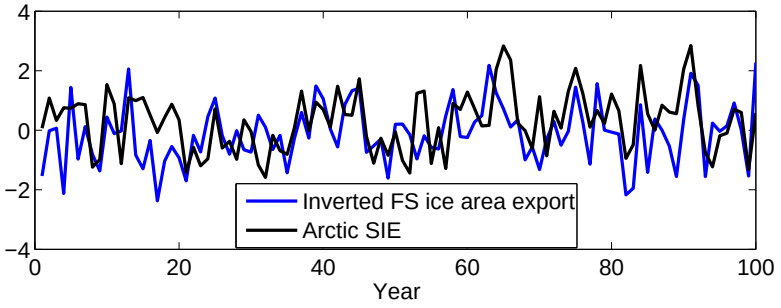

Figure 7. Spring (March–August) Fram Strait ice area export and September Artic SIE anomaly from the 3600 year long control simulation. Both time series are unfiltered and normalized by their standard deviations. Only the first 100 years is shown. The correlation between the two series is $r = -0.34$.

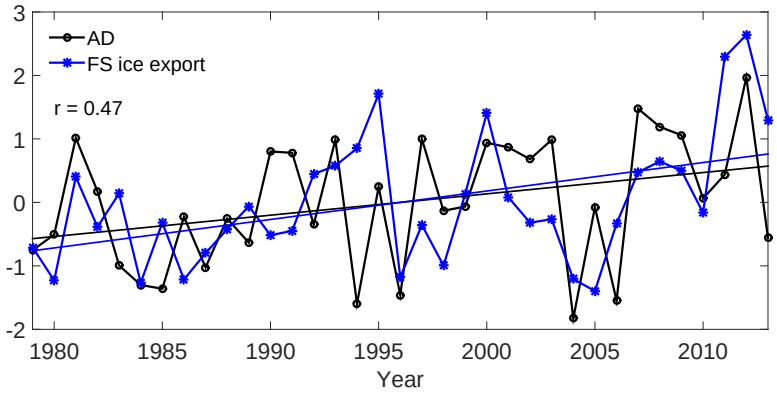

Figure 8. Observed March–August Fram Strait ice export and April–July Arctic Dipole (NCEP/NCAR reanalysis) anomalies from 1979–2013. Both time series are normalized by their standard deviations, 0.827 million km^2 and 31.7 hPa, respectively. The correlation is 0.38 when both time series are detrended (not shown).